Mechanical properties and thermal shock in thin ZrO_2-Y_2O_3-Al_2O_3 films obtained by the sol-gel method

Antonio Díaz-Parralejo[1]; M. Ángeles Díaz-Díez[1]; José Sánchez-González[1];

Antonio Macías-García[1*]; Juan Pablo Carrasco-Amador[2]

[1] *Department of Mechanical, Energy, and Materials Engineering. University of Extremadura.*
Avda de Elvas, s/n. 06006 Badajoz. Spain

[2] *Department of Graphic Expression. University of Extremadura.*
Avda de Elvas, s/n. 06006 Badajoz. Spain

Abstract: Thin multilayer coatings of ZrO_2-Y_2O_3-Al_2O_3 were prepared using the sol-gel method and dip-coating technique in order to advance in the study of what influence the incorporation of Al_2O_3 has on films of Y_2O_3-doped ZrO_2, investigating its role in the synthesis of the solutions and in the characteristics and properties of the coatings. After the characterization of the solutions used in the process, the microstructure of the films was studied and their mechanical behaviour and resistance to thermal shock were determined so as to optimize the characteristics and functionality of these coatings. With increased alumina content, 3YSZ-Al_2O_3 (20 mol%), the cubic phase of the zirconia disappeared completely at the sintering temperature used (700°C), resulting in the tetragonal phase with Al in solution. There was also a decrease in the coatings' hardness and Young's modulus, and an increase in toughness and resistance to thermal shock. These results allow guidelines to be established for the design of multilayer structures that are, tougher, more resistant, and have improved surface properties.

Keywords: thin films; dip-coating; zirconia; mechanical behaviour; thermal shock.

* Corresponding author: Antonio Macías-García, PhD
E-mail: amacgar@unex.es / Tel.: +34 924 289 600 / Fax: +34 924 289 601
University of Extremadura. School of Industrial Engineering. Avda de Elvas, s/n. 06006 Badajoz (Spain).

1. INTRODUCTION

Surface protection using ceramic coatings is an excellent option for their interesting physicochemical properties and high-temperature stability, rigidity, and resistance to wear and tear [1-3] in technological applications in which materials operate in aggressive environments or under extreme conditions of temperature or pressure. In particular, the manufacture of materials covered with base layers of zirconia (ZrO_2) have prompted numerous investigations due to their interesting properties and applications in various technological fields.

The sol-gel process is one of the most interesting options for obtaining thin films of oxides, and there are multiple examples in the literature that illustrate its versatility and simplicity [4, 5]. In addition, this method has certain advantages over other techniques, such as low processing temperatures, precise control of chemical composition, excellent adhesion to substrates, etc. The immersion method, *dip-coating*, is a deposition technique used to obtain coatings that has some advantages such as the ability to cover large surfaces, the simplicity of the equipment needed, and low cost.

The performance of sol-gel coatings depends to a large extent on their structural quality, since the presence of cracks and pores degrades their mechanical properties, and hence their effectiveness as protection [6]. For this reason, it is very important to control the degree of densification of the coatings during the different stages of the process. Another point of great technological importance to highlight is control of the coating's thickness, *d*, which depends on properties of the sol-gel solution (density, viscosity, etc.) and the actual deposition process (withdrawal rate of the substrate from the sol-gel solution). It is important to note that the thicker the coating, the greater the degree of chemical, thermal, and mechanical protection the substrate will offer.

The aforementioned two aspects, structural quality and maximum thickness, are sometimes difficult to reconcile. A certain limiting value inevitably results in the appearance of cracks in the coating which degrade its efficiency as a protective barrier. This gives rise to the notion of maximum thickness limit, called the critical thickness, t_c, and defined as the maximum coating thickness free of cracks that can be obtained in a single deposition process (monolayer coating). Nonetheless, it is possible to obtain coatings free of cracks with thicknesses greater than the critical thickness by depositing successive layers (multilayer coating). This method involves repeating the monolayer process as many times as suggested by the ratio between the desired thickness, t, and t_c. To manufacture multilayer coatings, it is advisable to determine t_c and the necessary experimental conditions beforehand. This will make it possible to ensure that all the layers are free of cracks and maximize the process of obtaining coatings of several layers.

The controlled design of zirconia-based sol-gel coatings is a challenge of major technological significance due to the interesting physicochemical properties of these materials [7], as well as the aforementioned advantages of the sol-gel method itself. However, one of the properties that partly limits their applicability is low resistance to thermal shock. When the surface of a ceramic material is subjected to a sudden change in temperature, this produces stresses that can cause it to rupture. These stresses arise due to differential expansions induced during the application of a specific temperature gradient. These can also form in polycrystalline or multiphase materials due to differential expansions between adjacent phases or grains [8].

The sensitivity of a material to these deformations determines its resistance to sudden changes in temperature. Therefore, a material's response to thermal shock depends on its mechanical and thermal properties. To assess the stresses induced by thermal shock, one needs to consider a great number of parameters such as Young's modulus, Poisson's ratio,

the coefficient of thermal expansion, the thermal conductivity of the material, the size and shape of the sample, and those that refer to the characteristics of the tempering treatment such as the temperature gradient and heat transfer coefficient of the medium in which the heat is produced [9-10].

Various parameters have been developed to assess the thermal shock of ceramic materials, many of them introduced by Hasselman [11], among which are the coefficient of thermal expansion, elasticity, and mechanical resistance. Tancret and Ostertock [12] have recently proposed that one of these parameters be used to study ceramic materials with cracks produced by indentation. The main advantage of using indentation cracks is that, contrary to other methods where a great number of parameters need to be known to assess resistance to thermal shock, one only needs to know the development of the fissures.

In order to improve the mechanical, thermal, and chemical protection properties of ZrO_2 coatings, researchers have tested various compositions and proportions of certain oxides to use as dopants, such as Al_2O_3, MgO, etc. [13-15]. The present work seeks to obtain and characterize multilayer coatings with a ZrO_2 and ZrO_2-Al_2O_3 base through the use of the sol-gel method and dip-coating technique to study the effect of a wide range of $\%Al_2O_3$ (between 0-20 $\%Al_2O_3$) incorporated into the coatings on their micro-structural and mechanical properties and their behaviour when confronted with thermal shock. The intention is to establish guidelines to follow when designing multilayer structures that are tougher, more resistant, and have better surface properties.

2. EXPERIMENTAL METHOD

2.1. Preparation and characterization of stable solutions

The starting solution was prepared by mixing and stirring zirconium (IV) n-propoxide (ZNP) 70 wt.% diluted in propanol (PrOH) and with nitric acid (HNO_3) as catalyst in an

anhydrous nitrogen atmosphere to avoid hydroxide precipitation. To prepare precursor solutions for 3 mol% yttria-stabilized zirconia (3YSZ), the starting solution was mixed with a second solution of yttrium (III) acetate ($YAc{\cdot}4H_2O$) dissolved in PrOH and HNO_3. The ZNP/PrOH/H_2O/HNO_3 molar ratios of the final solution were 1/15/6/1 [13].

The Al_2O_3 sol was prepared by mixing aluminium tri-sec-butoxide with propanol, then adding HNO_3 as catalyst. The aluminium tri-sec-butoxide/propanol/H_2O/HNO_3 molar ratio was 1/15/6/1. The alumina sol was added into the 3YSZ sol under continuous stirring for 1 h to prepare 3YSZ-Al_2O_3 (5 mol%) and 3YSZ-Al_2O_3 (20 mol%) coating solutions.

The 3YSZ, 3YSZ-Al_2O_3 (5 mol%), and 3YSZ-Al_2O_3 (20 mol%) sols were characterized by measuring their density and viscosity at room temperature, using a 10-mL Gay-Lussac pycnometer for liquids and a modified Ostwald viscometer, respectively (see Table 1). The solution pH, measured by paper indicator (Acilit, Merck) was approximately 0.5 in all solutions. As expected, the prepared sols were stable, clear, and transparent.

=== TABLE 1 ABOUT HERE ===

2.2. Preparation and characterization of the coatings

AISI 310 stainless steel (Fe/Cr25/Ni20) sheets of dimensions 75 × 25 × 1 mm were used as substrate. To increase and facilitate the coatings' adhesion, these stainless steel pieces were first mechanically modified by sanding, polishing, and a final thermal treatment at 300°C in air for 1 h. Soda-lime glass sheets with the same dimensions were used as transparent substrates to determine the thickness of the films by means of transmittance spectra in accordance with the previously reported procedure [13]. All of them were cleansed before use with dilute acetic acid solution, distilled water, and 96% ethanol.

The prepared sols were deposited onto the substrates at room temperature by dip-coating by means of a HOYTON HM-20D electromechanical testing machine using different withdrawal rates (4–14 cm/min). Finally, the coated substrates were air-dried at 100°C for 1 h, at ambient pressure. The dried coated substrates were annealed (sintered) at different temperatures depending on the substrate employed (500°C for soda-lime glass substrates and 700°C for AISI-310 stainless steel substrates) using a quartz-tube furnace with a heating-cooling rate of 3°C/min and soaking time of 2 h under air atmosphere. The procedure for obtaining multilayer coating films involved from 3 to 5 repetitions of the above consecutive stages.

A standard Spectronic Helios Alpha UV–Vis spectrophotometer (Thermo Fisher Scientific) was used over the spectral range of 200-1000 nm to analyse the $ZrO_2/Y_2O_3/Al_2O_3$-based monolayer and multilayer films coated onto transparent substrates, determining the refractive index and transmittance curves of the different coatings. The porosity of the coatings and thickness they reached using different withdrawal rates were determined by applying Swanepoel's method [16]. A Nikon reflected-light optical microscope (Epiphot 300) was used to assess the structural quality and check for the presence of possible fissures and cracks in the $ZrO_2/Y_2O_3/Al_2O_3$-based monolayer and multilayer films. The XRD pattern was obtained using a Philips PW-1800 powder diffractometer with CuK_α radiation (λ = 1.54183 Å) and a secondary graphite monochromator with generator settings of 40 kV and 35 mA. The diffraction data were collected over a 2θ range of 20–80° with a step width of 0.02° and a counting time of 5 s/step. A Nicolet Almega Dispersive Raman spectrometer (Thermo Scientific) has been used. The spectra have been obtained with a 633 nm laser at 100% power, with fluorescence correction and subsequently applying a smoothing.

The mechanical responses of the uncoated and the zirconia and zirconia-alumina coated steel samples were studied using a Berkovich (three-sided pyramid) indenter at loads of 5 mN to 20 mN, obtaining the values of ultra-microhardness (*H*) and Young's modulus (*E*) from the indentation load–unload curves (load versus penetration depth) [17].

The coating materials are ceramics with a relatively high coefficient of expansion and toughness. Applying a Vickers indenter to their surface creates imperfections in the form of indentations from whose vertices appear what are known as Palmqvist cracks [18]. To study the response to thermal shock, indentations were made with a Shimadzu Micro Hardness Tester Type M Vickers indenter, applying a load of 5 N to induce residual stresses which are responsible for the expansion of the cracks during the indentation process. Different temperature gradients were applied (550-20°C, 400-20°C and 300-20°C), and different cooling media and curves: abrupt cooling in water at room temperature at a cooling rate of around 300°C/s; cooling inside the oven (Figure 1) at a cooling rate of 0.7 °C/s for the first 240 s, and then approximately 0.2°C/s; air cooling (Figure 2) with a cooling curve of two well-differentiated parts – first, a relatively fast and strong cooling rate of about 35 °C/s for 10 s, and then, starting from 10 s, a second cooling phase at an approximate rate of 1° C/s when the sample was in contact with air. A Flir Systems InfraCAM thermal imaging camera, and a GM 900 infrared thermometer were used to check the temperatures.

=== FIGURE 1 ABOUT HERE ===

=== FIGURE 2 ABOUT HERE ===

3. RESULTS AND DISCUSSION

To obtain coatings with good structural quality using the dip-coating technique, we first needed to determine the maximum withdrawal rate in the deposition stage allowing us to

obtain the thickest possible coatings without cracks. This withdrawal rate depends on the physicochemical properties of the solutions used, especially their viscosity [13]. Therefore, for practical purposes and due to the aging of the solutions over time, the product resulting from multiplying the maximum withdrawal rate by its viscosity needed to be determined ($v_{max} \times \eta$). This product (see Table 1) remained constant over the time of use of the fresh solutions, i.e., without excessive aging time. The values showed a decrease as the Al_2O_3 content of the compositions increased, which led us to use slower withdrawal rates in the deposition processes and thus obtain slightly smaller thicknesses for each layer of coating deposited.

Once the optimal conditions for the coating had been determined in accordance with the withdrawal rate and viscosity, the coatings were made under the conditions set out in Table 1. Micrographs resulting from the above process are shown in Figure 3. In particular, Figures 3a and 3b show the micrographs of coatings deposited onto soda-lime glass and AISI-310 stainless steel substrates, respectively, that indicate the start and appearance of cracks resulting from a withdrawal rate slightly greater than the critical value, and Figures 3c and 3d the respective major progressive cracking resulting from the use of a withdrawal rate very much greater than the critical value. It should be noted that these cracks do not disappear with the application of subsequent deposition layers. Therefore, it is especially important to be careful not to exceed this critical deposition rate for each layer.

=== FIGURE 3 ABOUT HERE ===

Once the critical deposition rate had been set and the coatings made, different parameters of the coatings were determined by UV-visible spectrophotometry. Figure 4 shows the transmittance curves of monolayer films obtained from sols 3YSZ, 3YSZ-Al_2O_3 (5 mol%), and 3YSZ-Al_2O_3 (20 mol%) coated onto a soda-lime glass substrate employing a

withdrawal rate of 14 cm/min and heat-treated at 500°C. The presence of a greater number of peaks and interference bands, as well as the greater amplitude of these bands, it should be interpreted as that the sample will present higher densification (approximation to the theoretical refractive index, *n*, as well as a lower porosity, *P*), even also a greater film thickness. However, the final value of such parameters will also be conditioned by the relative positions (wavelength of max/min) at which these peaks appear. Therefore, a thorough analysis of these transmittance curves is essential. From the transmittance curves and applying Swanepoel's method, it is possible to obtain the coating's refractive index, *n*, thickness, *t*, and porosity, *P* [13, 16]. The results are presented in Table 2 (the estimated errors are around 3%). A slight decrease in the thickness of the films is observed, as well as a lower densification as the $\%Al_2O_3$ increases in the samples.

=== FIGURE 4 ABOUT HERE ===

=== TABLE 2 ABOUT HERE ===

The phases present in the coatings were analysed by X-ray diffraction. Figure 5 shows the experimental XRD pattern obtained from each of the coatings used in this study and deposited onto AISI-310 stainless steel substrates. Peaks appear in the austenitic phase of the substrate (γ-Fe), while the other peaks correspond to the cubic phase of zirconia (c-ZrO_2) and in smaller measure to its tetragonal phase (t-ZrO_2). The main X-ray diffraction peaks of c-ZrO_2 (with 3mol% Y_2O_3 as stabilizing oxide) are the Miller indices 111, 200, 220, 311 and 400, which in a typical Cu Kα incident radiation experiment appear at the positions angle 30.2, 35.0, 50.4, 59.8 and 74.0 º2θ, respectively. The quantitative analysis of the XRD data (Table 3) showed the cubic phase of the zirconia to be present in the 3YSZ and 3YSZ-Al_2O_3 (5 mol%) coatings, with the latter having a greater presence of a tetragonal phase of zirconium oxide appearing in stable form. On the other hand, in the

3YSZ-Al_2O_3 (20 mol%) coating samples, the cubic phase of zirconia had disappeared, giving way to the tetragonal phase of zirconia and its tetragonal phase with aluminium in solution. The calculated crystallite size, *D*, corresponds to homogeneous regions of the coating that produce coherent diffraction, and not necessarily to the grain or crystal size which typically is greater. It has to be noted that we tried to calculate the mean quadratic micro-deformation, e^2, but determined that it was impossible since the partition factor of the pseudo-Voigt function (function used to fit the diffractograms) was greater than 0.328.

=== FIGURE 5 ABOUT HERE ===

The crystallite size implies the presence of different regions and borders within the grain of the material, and consequently entails a certain discontinuity in its crystalline structure that prevents or hinders certain phenomena such as the movement of dislocations, the propagation of fissure tips, etc. This constitutes a mechanism for strengthening the material.

=== TABLE 3 ABOUT HERE ===

The result of the presence of the cubic phase of zirconia was somewhat unexpected since previous works about sol-gel powders have suggested a tetragonal structure or some uncertainty between the tetragonal and cubic phases for similar contents of yttria [19, 20]. However, we would argue that the crystalline structure of the zirconia coatings obtained via the sol-gel method does not depend exclusively on the yttria content as is the case in traditional sintering of zirconia from particles, but rather on a wide range of factors such as drying rate, the pH of the solution, areas under compression stress, etc. [21].

In order to confirm the crystalline structure of the sample, the Raman spectrum of the 3YSZ coating was obtained and shown in Figure 6. Basahel et al. [22] reported that the Raman spectrum for c-ZrO_2 is characterized by a band at 145 cm^{-1}, a broad bands

centered at 246, 301, 436 and 625 cm^{-1}, and a strong band between 607 and 617 cm^{-1}. Likewise, the t-ZrO_2 shows peaks at 149, 224, 292, 324, 407, 456 and 636 cm^{-1}. Therefore, Raman spectroscopy indicates that the 3YSZ sample shows bands that correspond to a combination of both types of phases. Although X-ray diffraction did not show this clearly, probably due to the overlap of the diffraction peaks.

=== FIGURE 6 ABOUT HERE ===

To study the mechanical behaviour of the coatings, ultra-microhardness tests were carried out. Figure 7 shows the experimental Berkovich load/penetration depth curves corresponding to a load of 20 mN for the different composition coatings used in this work. For comparison, also presented are the AISI-310 stainless steel substrate curve to make it easier to appreciate the reinforcing effect of the coatings, and the curve obtained for a massive zirconia sample to show its similarity and proximity to that of the coating of zirconia without added alumina.

=== FIGURE 7 ABOUT HERE ===

Nonetheless, the large penetration depths reached in these experiments relative to the thickness of the coatings (400-500 nm) mean that one can argue that the substrate clearly contributes to the observed mechanical response of the samples [23, 24]. Therefore, to obviate the effect of the substrate and obtain the exclusive properties and mechanical response of each coating, we carried out ultra-microhardness tests with loads of 5 mN (see Figure 8). From these tests, we obtained values for the coatings' hardness, *H*, and Young's modulus, *E*. The results are presented in Table 4 (the estimated errors are around 3%).

=== FIGURE 8 ABOUT HERE ===

=== TABLE 4 ABOUT HERE ===

These results indicate a significant progressive decrease in the coatings' surface hardness and Young's modulus with increasing amounts of alumina in solution. Although this result was somewhat unexpected a priori, it does not necessarily have to be associated with a decrease in the coatings' mechanical properties since, although it certainly causes a reduction in their hardness, it also leads to an increase in their toughness. Basically, the results can be attributed to three effects. One is that the porosity of the layers or multilayers increases as the alumina content of the coatings increases for sintering in the range 500-700°C [13]. Another is that, at these thermal treatment temperatures, there is still no clear presence or formation of alumina compounds in the coatings, as shown by the quantitative X-ray analyses. And a third is the qualitative fact that the densification of crystalline coatings necessarily implies the activation of diffusion mechanisms which will logically only be effective at sufficiently high temperatures (approximately greater than 0.4 times the fusion temperature) [25].

In order to analyse the response of the coatings to thermal shock, optical micrographs were obtained after abruptly cooling them in water from 550°C to 25°C. Figure 9 shows these micrographs after the creation of indentations with the Vickers indenter at a 5 N load. The images show that there are fewer cracks and less growth in the 3YSZ-Al_2O_3 (mol20%) coatings, Figure 9(c), than in the 3YSZ and 3YSZ-Al_2O_3 (mol5%) coatings, Figures 9(a) and 9(b), respectively.

These results indicate greater resistance to the propagation of the cracks in the coatings as the presence of Al_2O_3 in solution increases. This is consistent with both the mechanical properties determined in the ultra-microhardness tests and the presence of the zirconia tetragonal phase. Effectively, the progressive reduction of hardness and elastic modulus of the coatings as the presence of Al_2O_3 in solution increases leads to a decrease in

fragility and increase in toughness. Likewise, it is well known that when the metastable tetragonal phase is present it is susceptible to a martensitic transformation to the monoclinic phase driven by the crack propagation energy, causing an increase in volume at the fissure tip that compresses the area and prevents propagation of the cracks [26]. Similarly, the decrease in crystallite size as the proportion of Al_2O_3 increases leads to the presence of more borders and discontinuities in the granular structure of the coatings, and this translates into a greater number of obstacles to the advance and propagation of the fissure tips, thereby increasing the toughness of the material. All this is reflected in the values of the stress concentration factor, K_{IC} (Table 4), which determine the material's fracture toughness, with resistance against the propagation of cracks.

=== FIGURE 9 ABOUT HERE ===

The cracks propagate irregularly and multi-directionally around the indentation areas, and the greater presence of micro-cracking near the vertices of the indentation is very likely to be associated with the relaxation of residual stresses that accumulate during the drying and sintering stages of these coatings [27]. On the one hand, the volumetric expansion that occurs when the micro-cracks appear tends to close the faces of the cracks during their propagation, and on the other, the appearance of this type of crack leads to a decrease in the elastic modulus in the cracked area, making it more deformable and less rigid than the rest of the material. Nonetheless, there is a limit to this reinforcing mechanism, so that, from a certain density of micro-cracks onwards, a crack can propagate more easily through this area [28, 29].

The results of the experiments carried out with different heat steps (400°C-25°C and 300°C-25°C) again showed a behaviour of the coatings similar to that of the heating to 550°C discussed above, with the number and growth of the cracks decreasing as the thermal gradient is smaller. In the experiments involving thermal shocks with different

curves or cooling media (air cooling or cooling inside the oven), we observed that the damage produced and the growth of the induced cracks were very similar in behaviour to the case of cooling in water. This demonstrates that these materials are affected more by the thermal step or gradient to which they are subjected than by the medium in which the cooling takes place or by its severity as long as the temperatures are within the moderate range that we tested.

4. CONCLUSIONS

Based on the experiments and analyses carried out in this work, we can draw the following principal conclusions:

- The different precursor solutions of ZrO_2-Y_2O_3-Al_2O_3 prepared allow transparent, low viscosity solutions to be obtained that are ideal for the formation of homogeneous coatings on soda-lime glass and AISI-310 stainless steel substrates with sintering at temperatures between 500°C and 700°C.
- The 3YSZ and 3YSZ-Al_2O_3 (5 mol%) coatings exhibit a crystalline structure comprising zirconia in the cubic phase (*c*-ZrO_2) and, to a lesser degree, the tetragonal phase (*t*-ZrO_2) with Al in solution also present in stable form. At the greater alumina content, 3YSZ-Al_2O_3 (20 mol%), the cubic phase of zirconia disappears completely, leaving its tetragonal phase with Al in solution.
- The increase in alumina content in the coatings causes significant changes in the material's mechanical and thermal properties, affecting its mechanical resistance, toughness, and response to thermal shock. Progressive decreases in hardness, *H*, and Young's modulus, *E*, and a slight increase in toughness of the treated coatings are observed. This fact is probably associated with the increase in porosity and the lack of sintering and densification of the aluminium oxide which would have required higher temperatures than those used in the present work.
- The thermal gradient to which the material is subjected in the thermal shock has a

decisive effect on its thermal behaviour as well as on the cracks generated and their propagation. At higher heating temperatures or with a large thermal step, the damage caused is greater, whereas the number of cracks and their growth decrease with declining thermal gradient. The curve or cooling medium used, however, has a limited effect on the appearance and development of the cracks, leading us to conclude that the thermal behaviour of these coatings is uninfluenced by the severity of the cooling medium as long as the temperatures used remain within the moderate range applied in the present study.

REFERENCES

[1] M. Atik, M.A. Aegerter, Corrosion-resistant sol-gel ZrO2 coatings on stainless-steel, J. Non-Cryst. Solids 147 (1992) 813-819.

[2] Y. Jiang, TY. Liu, HQ. Ru, et al., Ultra-high-temperature ceramic TaB2-SiC-Si coating by impregnation and in-situ reaction method to prevent graphite materials from oxidation and ablation, Ceram. Int. 45 (5) (2019) 6541-6551.

[3] H. Dislich, Sol-Gel Technology for Thin Films, Fibers, Performs, Electronics and Specialty Shapes, LC. Klein (Noyes, N. J. 1988) p51.

[4] V. Encinas-Sánchez, A. Macías-García, M.A. Díaz-Díez, A. Díaz-Parralejo, Characterization of sol-gel coatings deposited on a mechanically treated stainless steel by using a simple non-destructive electrical method, J. Ceram. Soc. Jpn. 124 (3) (2016) 185-191.

[5] T. Yamada, R. Okuda, H. Hirakoso, H. Kozuka, Sol-gel preparation of yttria-stabilized zirconia thin films and transfer to polycarbonate substrates, J. Sol-Gel Sci Tech. 92 (3) (2019) 554-561.

[6] P.D. Neto, M. Atik, L.A. Avaca, M.A. Aegerter, Sol-gel coatings for chemical protection of stainless steel, J. Sol-Gel Sci. Technol. 2 (1-3) (1994) 529-534.

[7] R. Pascual, M. Sayer, G. Yi, C. Baker, Phase-transformation kinetics in thin-film zirconia, J. Can. Ceram. Soc. 60 (2) (1991) 43-46.

[8] A.K. Stamper, D.W. Greve, T.E. Schlesinger, Deposition of textured yttria-stabilized ZrO2 films on oxidized silicon, Appl. Phys. Lett. 70 (4) (1991) 2046-2051.

[9] W.D. Kingery, Factors affecting thermal stress resistance of ceramic materials, J. Am. Ceram. Soc. 38 (1) (1955) 3-15.

[10] H. Chai, B.R. Lawn, Fracture mode transitions in brittle coatings on compliant substrates as a function of thickness J. Mater. Res. 19 (6) (2004) 1752-1761.

[11] D.P. Hasselman, Thermal stress resistance parameters for brittle refractory ceramics-A compendium, Am. Ceram. Soc. Bull. 49 (12) (1970) 1033-1037.

[12] F. Tancret, F. Ostertock, The Vickers indentation technique used to evaluate thermal shock resistance of brittle materials, Scripta Mater. 37 (4) (1997) 443-447.

[13] J.P. Carrasco-Amador, A. Díaz-Parralejo, A. Macías-García, M.A. Díaz-Diez, M. Olivares-Marín, Preparation and characterization of ZrO2/Y2O3/Al2O3 - based microstructured multilayer sol-gel coatings, Ceram. Int. 43 (16) (2017) 14210-14217.

[14] G. Pintilei, V. Crismaru, M. Abrudeanu, et al., The behavior of ZrO2/20%Y2O3 and Al2O3 coatings deposited on aluminum alloys at high temperature regime, Appl. Surf. Sci. 352 (2015) 178-183.

[15] T. Wang, J. Pu, C. Bo, L. Jian, Sol-gel prepared Al2O3 coatings for the applications as tritium permeation barriers, Fusion Eng. Des. 85 (2010) 1068-1072.

[16] R. Swanepoel, Determination of the thickness and optical-constants of amorphous-silicon, J. Phys. E: Sci. Instrum. 16 (12) (1983) 1214–1222.

[17] W.C. Oliver, G.M. Pharr, Nanoindentation in materials research: Past, present, and future, MRS Bull. 35 (11) (2010) 897-907.

[18] G. Fargas, D. Casellas, L. Llanes, M. Anglada, Resistance to thermal shock of Y-TZP with Palmqvist indentation cracks, J. Eur. Ceram. Soc. 26 (8) (2006) 1523-1524.

[19] S. Cengiz, M. Yazici, Y. Gencer, M. Tarakci, Characterization of coating formed on pure zirconium by MAO in yttrium acetate tetrahydrate containing electrolyte, Acta Phys. Pol., A. 127 (4) (2015) 1320-1325.

[20] K. Jiang, S.B. Liu, S. Wang, Phase stability and thermal conductivity of nanostructured tetragonal yttria-stabilized zirconia thermal barrier coatings deposited by air-plasma spraying, Ceram. Int. 43 (15) (2017) 12633-12640.

[21] J.C. Marrero, NFP. Ribeiro, C.F. Malfatti, MMV. Souza, Characterization of yttria-stabilized zirconia films deposited by dip-coating on La0.7Sr0.3MnO3 substrate: Influence of synthesis parameters, J. Adv. Ceram. 2 (1) (2013) 55-62.

[22] S.N. Basahel, M. Mokhtar, T.T. Ali, N. Katabathini, Influence of crystal structure of nanosized ZrO2 on photocatalytic degradation of methyl orange. Nanoscale Research Letters (2015) 10:73 2-13.

[23] W.C. Oliver, G.M. Pharr, Nanoindentation in materials research: Past, present, and future, MRS Bull. 35 (11) (2010) 897-907.

[24] S.K. Mishra, V. Kumar, S.K. Tiwari, et al., Development and degradation behavior of protective multilayer coatings for aluminium reflectors for solar thermal applications, Thin Solid Films 619 (2016) 202-207.

[25] M. Daroonparvar, MAM. Yajid, C.M. Kay, et al., Effects of Al2O3 diffusion barrier layer (including Y-containing small oxide precipitates) and nanostructured YSZ top coat

on the oxidation behavior of HVOF NiCoCrAlTaY/APS YSZ coatings at 1100 degrees C, Corros. Sci. 144 (2018) 13-34.

[26] P.B. Kirk, R.M. Pilliar, The deformation response of sol-gel-derived zirconia thin films on 316L stainless steel substrates using a substrate straining test, J. Mater. Sci. 34 (1999) 3967-3975.

[27] F. Tancret, F. Ostertock, The Vickers indentation technique used to evaluate thermal shock resistance of brittle materials, Scripta Mater. 37 (4) (1997) 443-47.

[28] Z. Li, B.L. Wang, K.F. Wang, L. Zheng, A multi-scale model for predicting the thermal shock resistance of porous ceramics with temperature-dependent material properties, J. Eur. Ceram. Soc. 39 (8) (2019) 2720-2730.

[29] P. Carpio, M.D. Salvador, A. Borrell, E. Sánchez, Thermal behaviour of multilayer and functionally-graded YSZ/Gd2Zr2O7 coatings, Ceram. Int. 43 (5) (2017) 4048-4054.

FIGURE CAPTIONS

Figure 1. Curve of cooling inside the oven, showing the section of temperatures from 550°C to 300°C.

Figure 2. Curve of cooling in air from 550°C to approximately the ambient temperature.

Figure 3. Optical micrographs of 3YSZ coatings deposited onto soda-lime glass (a, c) and AISI-310 steel (b, d), at withdrawal rates slightly greater than the critical (incipient cracks) and very much greater than the critical (completely cracked).

Figure 4. Transmittance curves of monolayer $ZrO_2/Y_2O_3/Al_2O_3$-based films obtained from sols and coated onto a soda-lime glass substrate, with a withdrawal rate of 14 cm/min and sintered at 500°C.

Figure 5. X-ray diffractograms obtained from 3YSZ (a), 3YSZ-Al_2O_3 (5 mol%) (b), and 3YSZ-Al_2O_3 (20 mol%) (c) coatings, deposited onto AISI-310 stainless steel substrates and sintered at 700°C.

Figure 6. Raman spectrum of 3YSZ sample.

Figure 7. Berkovich load/penetration depth curves carried out with a load of 20 mN on AISI-310 stainless steel, massive zirconia, and the 3YSZ, 3YSZ-Al_2O_3 (5 mol%) and 3YSZ-Al_2O_3 (20 mol%) coatings.

Figure 8. Berkovich load/penetration depth curves carried out with a load of 5 mN on 3YSZ, 3YSZ-Al_2O_3 (5 mol%), and 3YSZ-Al_2O_3 (20 mol%) coatings.

Figure 9. Optical micrographs at 500× of the Vickers indentations obtained in the 3YSZ (a), 3YSZ-Al_2O_3 (5 mol%) (b), and 3YSZ-Al_2O_3 (20 mol%) (c) coatings, showing the generation and propagation of cracks in the coatings after subjection to thermal shocks in

water from 550°C to the ambient temperature.

TABLES

Table 1. Characteristics of the prepared sols at 25°C.

Sol nomenclature	**Oxide concentration (g/L)**	**Density (g/cm^3)**	**Viscosity (cP)**	**v_{max} x η (cm/min x cP)**
3YSZ	77.6	0.885	5.1	85
3YSZ-Al_2O_3 (5 mol%)	73.0	0.890	6.3	70
3YSZ-Al_2O_3 (20 mol%)	62.8	0.898	5.5	60

Table 2. Product ($v_{max} \times \eta$), refractive index, n, critical thickness, t_c, and porosity, P, of the coatings used with an annealing temperature of 500°C.

Coating	**v_{max} x η (cm/min x cP)**	**n (λ = 600 nm)**	**t_c (nm)**	**P (%)**
3YSZ	85	1.98	200	24
3YSZ-Al_2O_3 (5 mol%)	70	1.86	190	30
3YSZ-Al_2O_3 (20 mol%)	60	1.78	185	33

Table 3. Quantitative analysis, crystalline phases present, and average crystallite size, *D*, in the coatings studied.

Coating	***c*-ZrO_2 (%)**	***t*-ZrO_2 (%)**	***t*-$AlZrO_2$ (%)**	***γ*-Fe (%)**	***D* (nm)**
3YSZ	92.6 ±2	-	-	7.4 ±1	23 ±2
3YSZ-Al_2O_3 (5 mol%)	17.1 ±2	-	38.0 ±2	44.9 ±2	12 ±2
3YSZ-Al_2O_3 (20 mol%)	-	18.9 ±2	65.8 ±2	15.3 ±2	11 ±2

Table 4. Mechanical properties (Berkovich test with 5 mN load and conventional test).

Sample	**Berkovich**		**Conventional**		K_{IC}
	***H* (GPa)**	***E* (GPa)**	***H* (GPa)**	***E* (GPa)**	**(MPa $m^{1/2}$)**
ZrO_2	12	220	12	220	-
3YSZ	10	190	-	-	1.50
3YSZ-Al_2O_3 (5 mol%)	8	170	-	-	1.94
3YSZ-Al_2O_3 (20 mol%)	6.5	160	-	-	2.82
AISI-310	2	200	2	200	-

*Declaration of Interest Statement

Antonio Macías-García, PhD
School of Industrial Engineering
University of Extremadura
Avda. de Elvas, s/n.
06006. Badajoz (Spain)
amacgar@unex.es

July 24, 2020

Editor
Ceramics International

Subject: Declaration of Interest Statement

Dear Editor,

The manuscript entitled "*Mechanical properties and thermal shock in thin films of the ZrO_2-Y_2O_3-Al_2O_3 system obtained by the sol-gel method*", demonstrate how an increase of alumina content in the coatings leads to significant changes in its crystalline structure and a decrease in the mechanical behavior and causes some changes in the intrinsic properties of the materials, which affect their thermal shock resistance.

Best regards,
Antonio Macías-García, PhD
University of Extremadura

Figure 1

Click here to download high resolution image

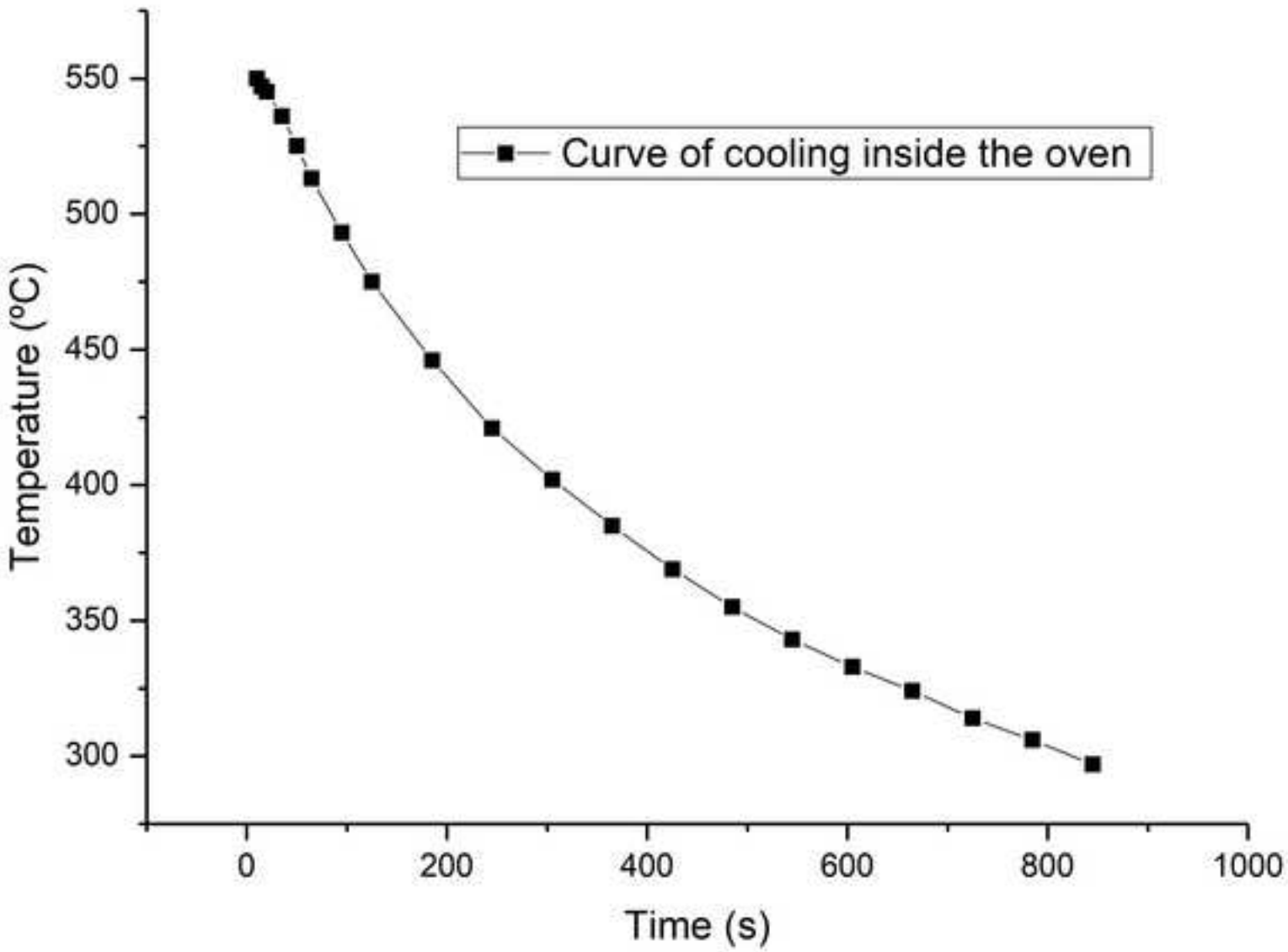

Figure 2

Click here to download high resolution image

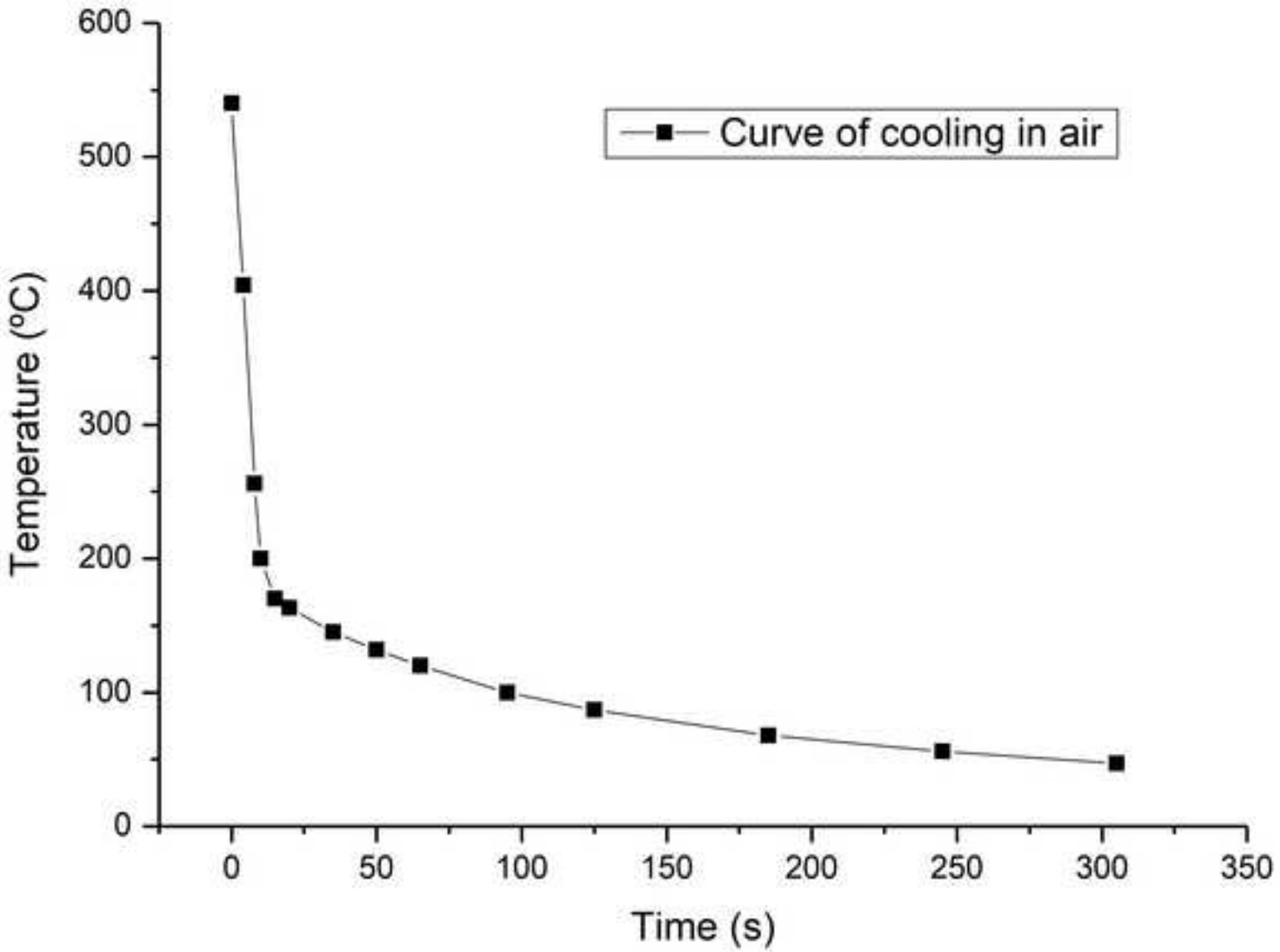

Figure 3

Click here to download high resolution image

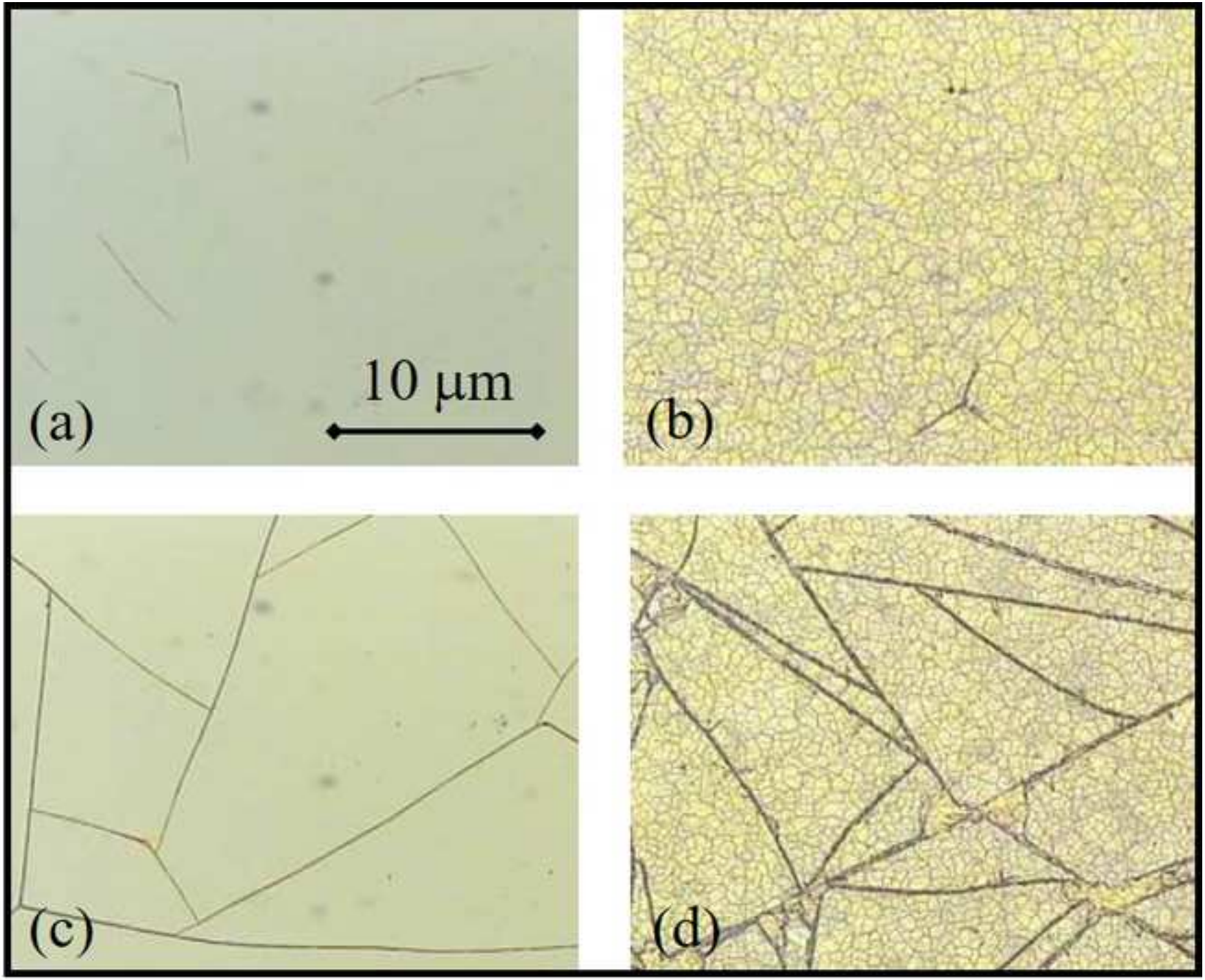

Figure 4
Click here to download high resolution image

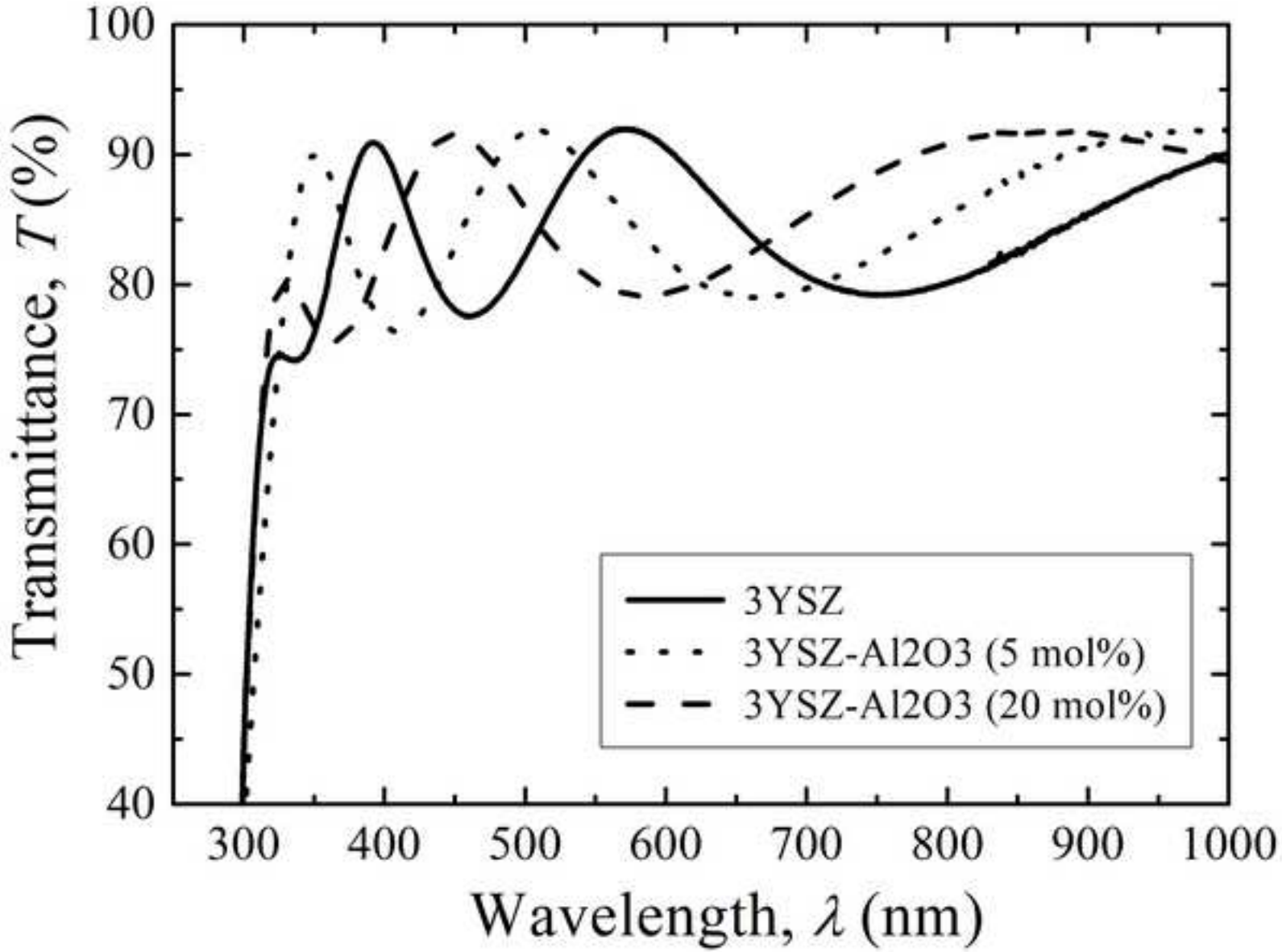

Figure 5

Click here to download high resolution image

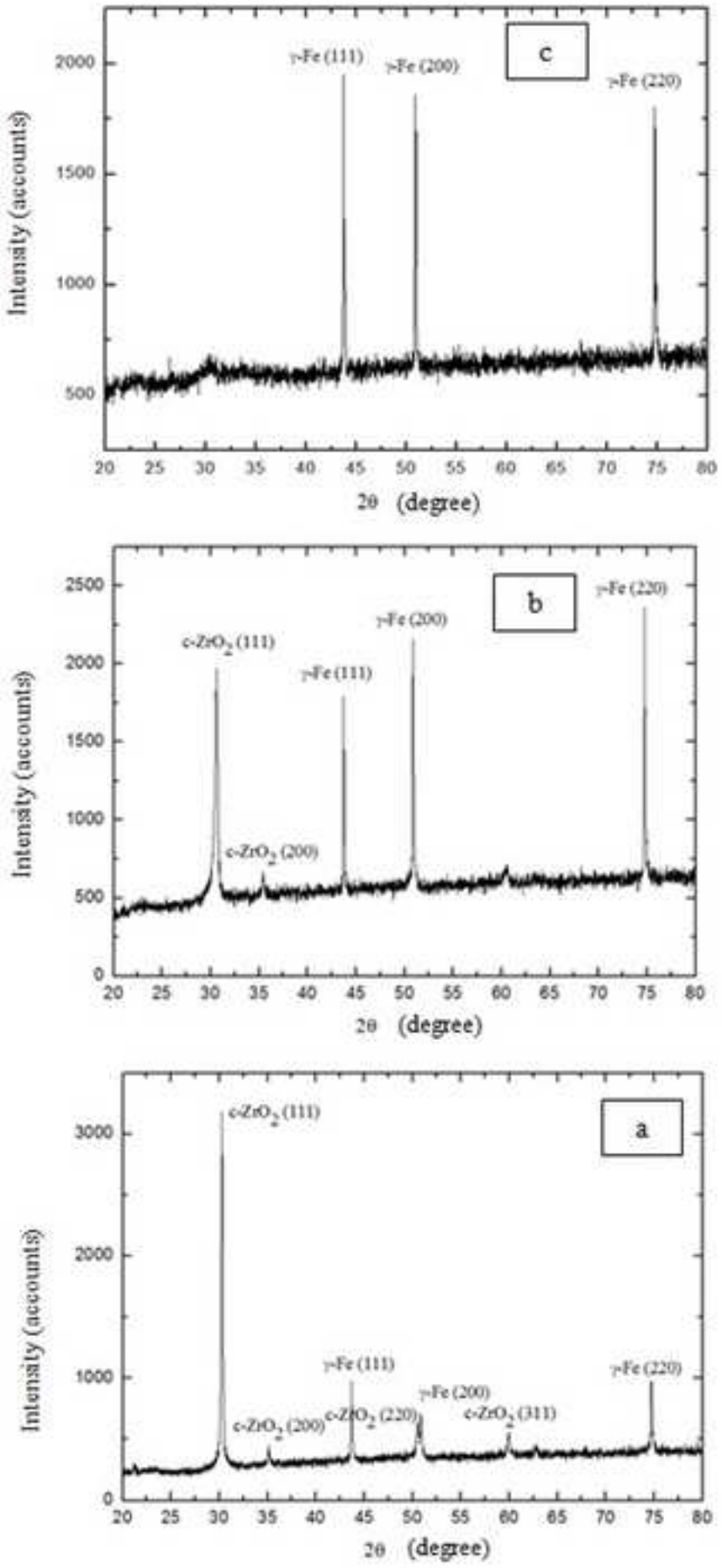

Figure 6

Click here to download high resolution image

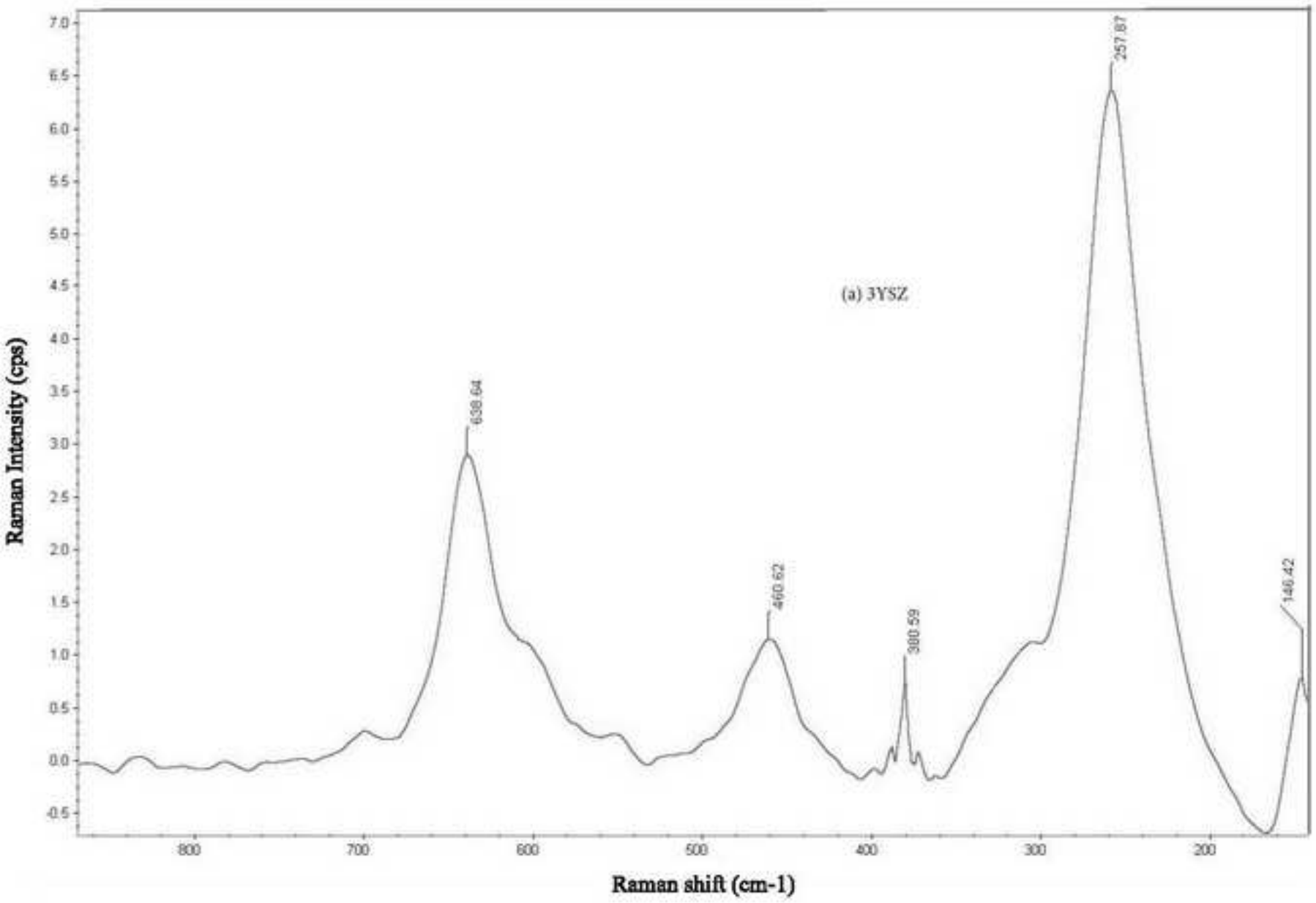

Figure 7

Click here to download high resolution image

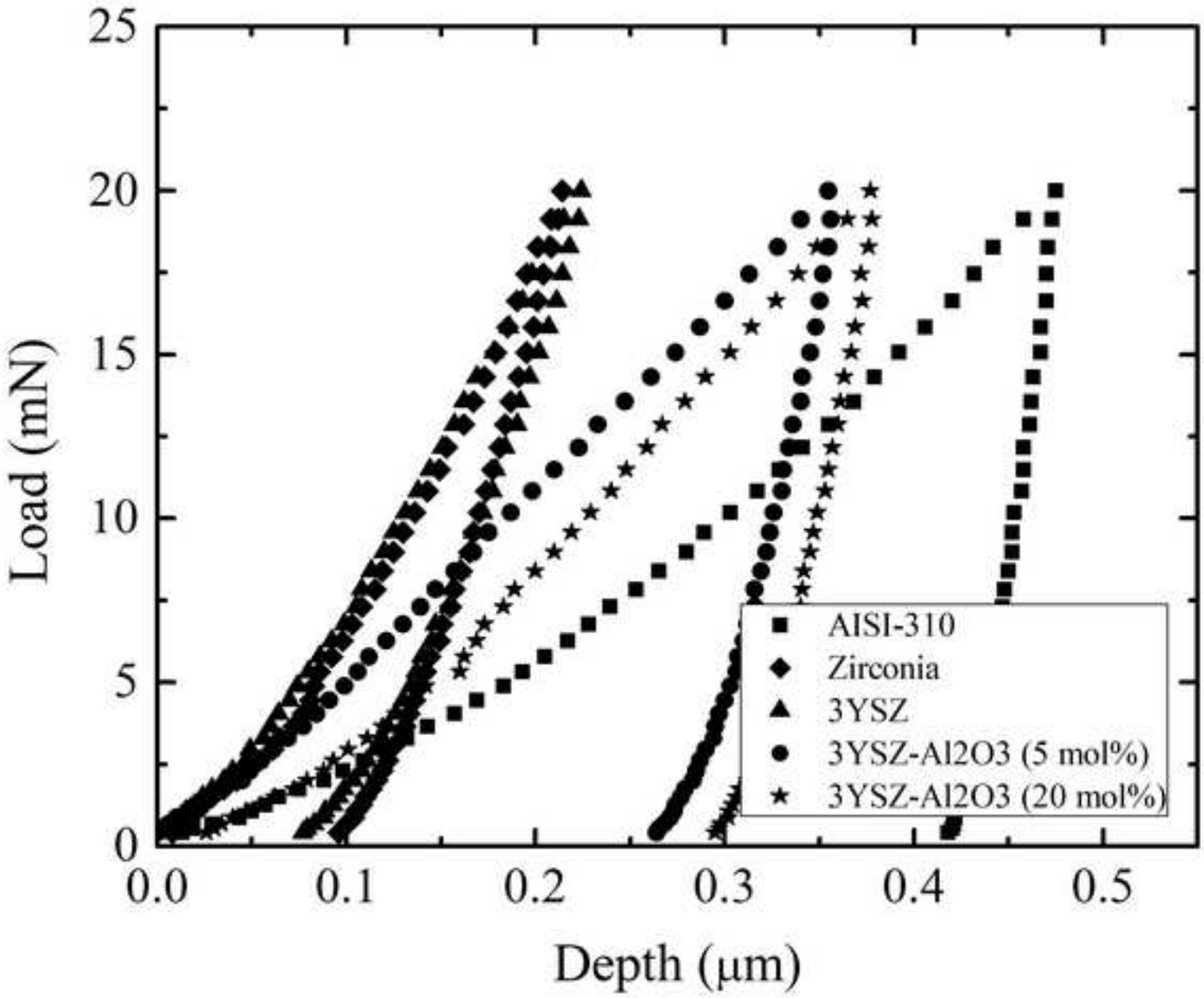

Figure 8

Click here to download high resolution image

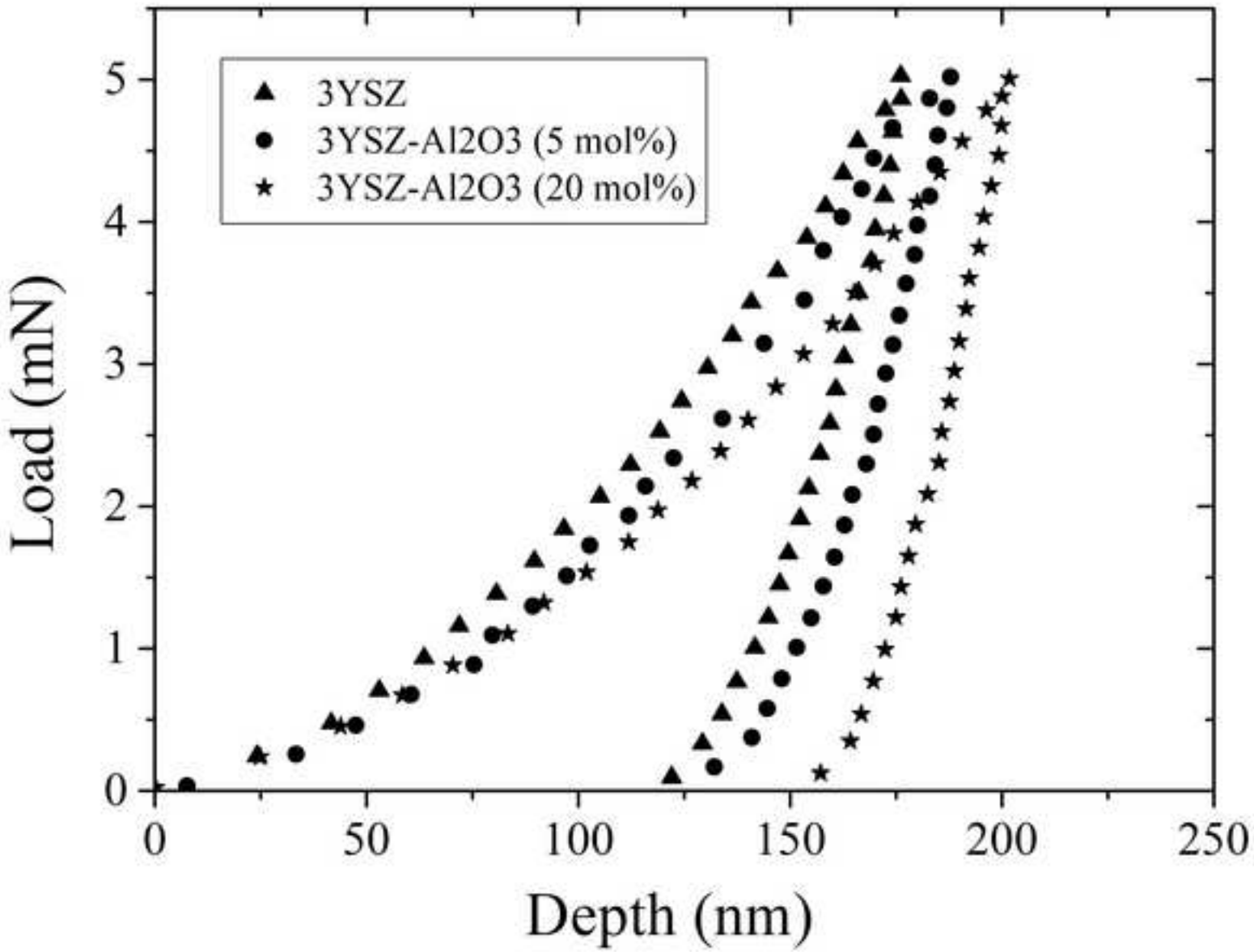

Figure 9
Click here to download high resolution image